Journal of Magnetics 17(2), 124-128 (2012) http://dx.doi.org/10.4283/JMAG.2012.17.2.124

Numerical Analysis of a Flux-Reversal Machine with 4-Switch Converters

Byoung-Kuk Lee[1] and Tae Heoung Kim[2]*

[1]*School of Information and Communication Engineering, Sungkyunkwan University, Suwon 440-746, Korea*
[2]*Department of Electrical Engineering, Engineering Research Institute, Gyeongsang National University, Gyeongnam 660-701, Korea*

(Received 22 February 2012, Received in final form 9 April 2012, Accepted 10 April 2012)

Many different converter topologies have been developed with a view to use the minimum number of switches in order to reduce construction costs. Among this research, the four-switch converter topology with a novel PWM control technique based on the current controlled PWM method is thought to be a good solution. In this paper, a two dimensional time-stepped voltage source finite-element method (FEM) is used to analyze the characteristics of a Flux-Reversal Machine (FRM) with a 4-switch converter. To validate the proposed computational method, a digital signal processor (DSP) installed controller and prototype FRM are built and experiments performed.

Keywords : brushless motor, converter, finite element method, flux-reversal machine, 4-switch

1. Introduction

As the principle of operation is similar to brushless DC machines (BLDCM), 3-phase Flux-Reversal Machines (FRM) need quasi-square current waveforms, which are synchronized with the back-EMF to generate constant output torque and have 120° conduction and 60° non-conducting regions. Also, at every instant only two phases are underway and the other phase is inactive. This control action can be realized using a 6-switch converter topology. A pulse width modulation (PWM) pattern for this converter is commonly used for the FRM to control the speed. However, these days, many different converter topologies have been developed to reduce the converter construction cost by using the minimum number of switches [1, 2]. One of them is 4-switch converter topology, which is shown in Fig. 1, with a novel PWM control technique based on the current controlled PWM method [3]. However, the FRM under a 4-switch converter is supplied by a different voltage level, $V_d/2$ or V_d at every instant, so that the load currents are reduced by a factor of $\sqrt{3}$ with respect to the current obtained when the same voltage and a 6-switch converter is used. Also, due to the voltage irregularity in the supply and lack of phase control freedom, the phase current can fluctuate, resulting in torque ripples. Therefore, when 4-switch FRM is used for certain applications, one should be able to understand and analyze the overall performance with respect to torque ripples and iron losses, compared with a 6-switch FRM.

In this paper, the authors introduce a computational method to analyze the characteristics of the FRM with a 4-switch converter using a two dimensional time-stepped voltage source finite-element method (FEM). To produce the 4-switch converter and perform the experiment, a digital signal processor (DSP) installed controller and prototype FRM were built. From the analysis and experimental results, it was verified that the proposed analysis method is suitable for analyzing FRMs with 4-switch converters.

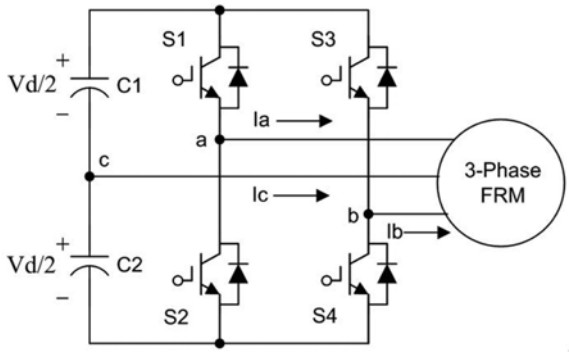

Fig. 1. 4-switch, 3-phase FRM drive systems.

*Corresponding author: Tel: +82-55-772-1717
Fax: +82-55-772-1719, e-mail: ktheoung@gnu.ac.kr

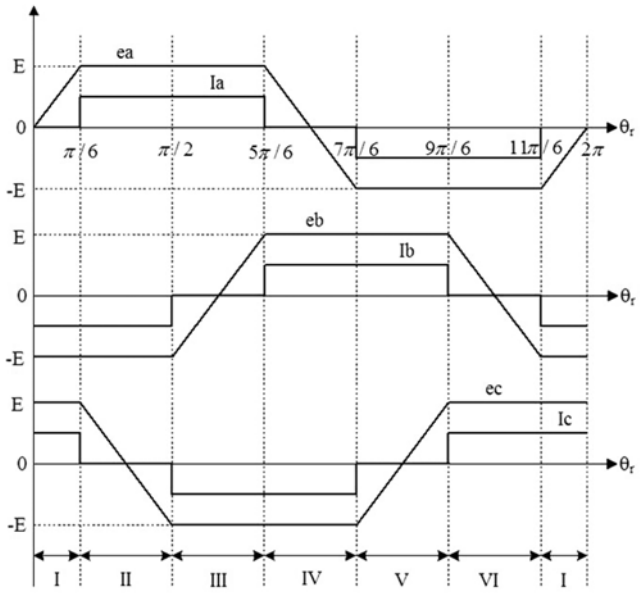

Fig. 2. Current profile of the 4-switch FRM drive.

2. PWM Algorithm for the 4-Switch Converter

In the 4-switch FRM, the three-phase currents should be synchronized with each counterpart back-EMF, so that the overall operation can be divided into six modes as shown in Fig. 2. As opposed to the 6-switch FRM, the 4-switch FRM converter can only generate four switching vectors: (0,0), (0,1), (1,0) and (1,1), where "0" means that the lower switch is turned on and "1" means the upper switch is turned on. With these four switching vectors, it is impossible to generate the proper current waveforms. Therefore, in this paper, a direct current controlled PWM algorithm is applied to generate the required speed-torque characteristics. The switching sequences of the 4-switch FRM drive are summarized in Table 1 and the detailed implementation of the direct current controlled PWM algorithm is depicted in Fig. 3 for each operation mode.

3. Finite Element Formulations

At each instant, the interaction between the 4-switch converter circuitry and electromagnetics is achieved by defining the winding current in terms of the electrical circuit parameters [4]. The actual phase currents of the 4-switch FRM are controlled by a hysteresis current controller. Therefore, detailed voltage equations taking account of current regulation using the hysteresis controller should be derived.

Table 1. Switching Sequences of the 4-Switch FRM Drives.

Modes	Active phases	Silent phases	Switching devices
Mode I	Phase B and C	Phase A	S4
Mode II	Phase A and B	Phase C	S1 and S4
Mode III	Phase A and C	Phase B	S1
Mode IV	Phase B and C	Phase A	S3
Mode V	Phase A and B	Phase C	S2 and S3
Mode VI	Phase A and C	Phase B	S2

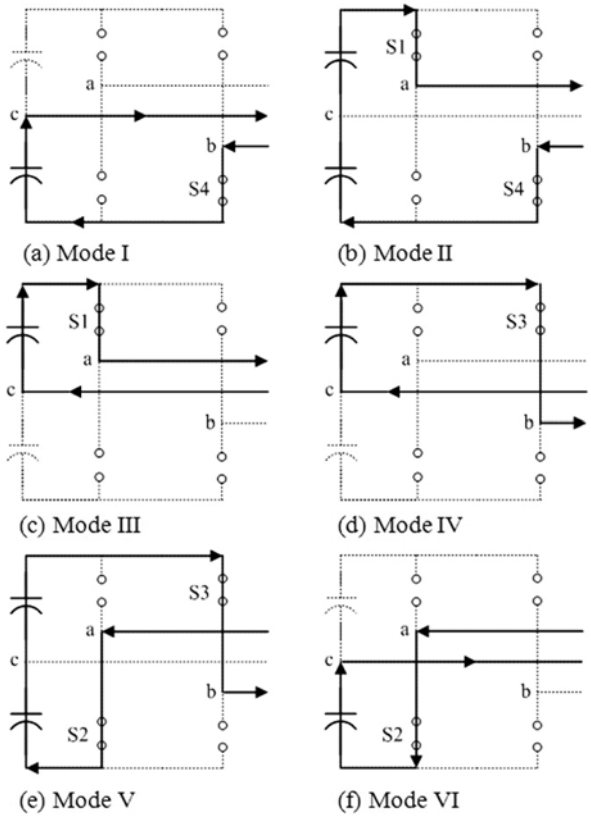

Fig. 3. Implementation of direct-current controlled PWM.

3.1. Voltage Equations in Mode I

With reference to Figs. 2 and 3(a), consider a 60-degree period when current is flowing through phases B and C. Switch S4 is turned on and off according to the current regulation in this mode, so the flow of current can be categorized into four cases as shown in Fig. 4. Fig. 4(a) and (b) show the current flows at the commutation instant when switch S4 is turned on and off, respectively. In these cases, the current continues to flow in open phase A due to its inductance L. As a result, two voltage equations can be written as:

$$R_c i_c + L_{lc}\frac{di_c}{dt} + \frac{d\Phi_c}{dt} + R_b i_b + L_{lb}\frac{di_b}{dt} - \frac{d\Phi_b}{dt} = V_1 \qquad (1)$$

$$R_c i_c + L_{lc}\frac{di_c}{dt} + \frac{d\Phi_c}{dt} + R_a i_a + L_{la}\frac{di_a}{dt} - \frac{d\Phi_a}{dt} = V_2 \qquad (2)$$

Where R is the resistance of the phase winding, L_l is the

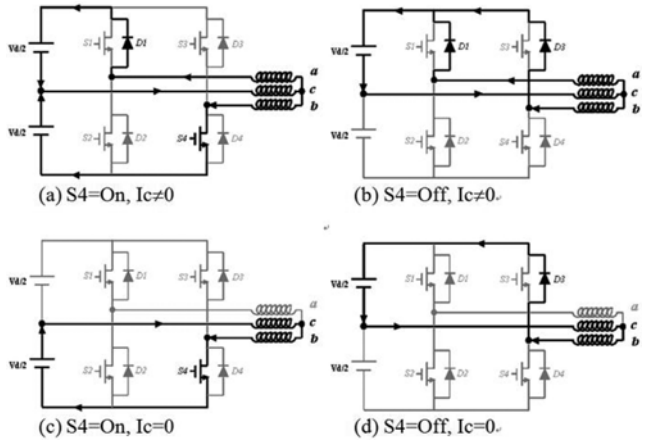

Fig. 4. The flow of current in Mode I.

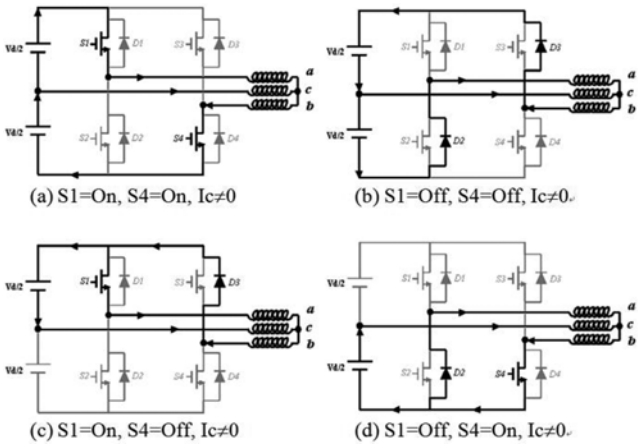

Fig. 5. The flow of current in Mode II (Ic≠0).

Table 2. Voltage Values in (1) and (2).

Case		*V1*	*V2*
Fig. 4	(a)	*Vd/2 -VCE*	*-Vd/2 -VF*
	(b)	*-Vd/2 -VF*	*-Vd/2 -VF*
	(c)	*Vd/2 -VCE*	
	(d)	*-Vd/2 -VF*	

leakage inductance of the stator coil ends and Φ is the flux linkage of the phase winding. V_1 and V_2 represent voltage and Table 2 shows the values. V_{CE} and V_F which are the forward voltage drop across the transistor and the diode, respectively.

If the current in open phase A decays to zero and switch S4 is turned on and off, only the main voltage equation exists as shown in Figs. 4(c) and 4(d). In these cases, the voltage equations are identical to (1).

3.2. Voltage Equations in Mode II

Special attention should be paid to mode II. In this mode, phases A and B are conducting the current and phase C is regarded as being unexcited, as such it is expected that there is no current in the phase C. However, the back-EMF of phase C can cause an additional and unexpected current, resulting in current distortion in phases A and B. Therefore, the back-EMF compensation needs to be considered [3]. If phases A and B are regarded as independent current sources, the influence of the back-EMF on phase C can be blocked and therefore cannot act as a current source, so that there is no current in phase C. This means that phase A and phase B currents should be sensed and controlled independently and the switching signals of S1 and S4 should be created independently. Accordingly, in this mode, the flow of current can be categorized into eight cases according to the new PWM control technique. Fig. 5 shows the flow of current at the commutation instant (phase C current continues to flow) when switches S1 and S4 are on and off. In these cases, the voltage equations can be written as follows:

$$R_a i_a + L_{la}\frac{di_a}{dt} + \frac{d\Phi_a}{dt} + R_b i_b + L_{lb}\frac{di_b}{dt} - \frac{d\Phi_b}{dt} = V_1 \qquad (3)$$

$$R_c i_c + L_{lc}\frac{di_c}{dt} + \frac{d\Phi_c}{dt} + R_b i_b + L_{lb}\frac{di_b}{dt} - \frac{d\Phi_b}{dt} = V_2 \qquad (4)$$

After the open phase C current decays to zero, any remaining current is caused by the back-EMF of phase C flows, as shown in Fig. 6, during the positive back-EMF period. The circuit voltage equations for each case can be written as follows:

$$R_a i_a + L_{la}\frac{di_a}{dt} + \frac{d\Phi_a}{dt} + R_b i_b + L_{lb}\frac{di_b}{dt} - \frac{d\Phi_b}{dt} = V_1 \qquad (5)$$

$$R_a i_a + L_{la}\frac{di_a}{dt} + \frac{d\Phi_a}{dt} + R_c i_c + L_{lc}\frac{di_c}{dt} - \frac{d\Phi_c}{dt} = V_2 \qquad (6)$$

As the current direction changes according to the polarity

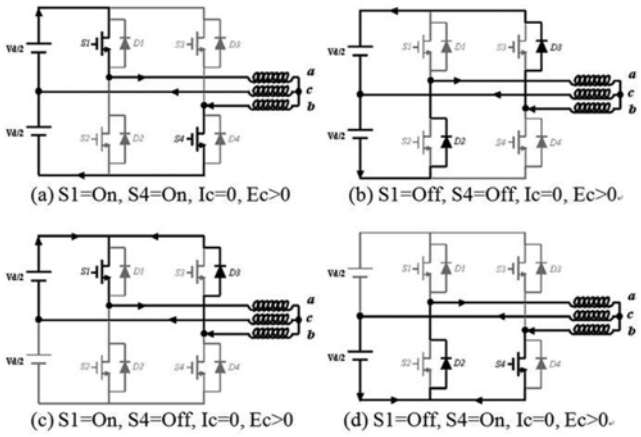

Fig. 6. The flow of current in Mode II (Ic=0, Ec>0).

Table 3. Voltage Values in (3), (4), (5), and (6).

Case		*V1*	*V2*
Fig. 5	(a)	*Vd -2VCE*	*Vd/2 -VCE*
	(b)	*-Vd -2VCE*	*-Vd/2 -VF*
	(c)	*-VF -VCE*	*-Vd/2 -VF*
	(d)	*-VF -VCE*	*Vd/2 -VCE*
Fig. 6	(a)	*Vd -2VCE*	*Vd/2 -VCE*
	(b)	*-Vd -2VCE*	*-Vd/2 -VF*
	(c)	*-VF -VCE*	*Vd/2 -VCE*
	(d)	*-VF -VCE*	*-Vd/2 -VF*

of the back-EMF, the flow of the current and voltage equations are identical to the case of Fig. 5 during the negative back-EMF period. Consequently, all voltage equations can be obtained. Table 3 shows the value of V_1 and V_2 in (3), (4), (5), and (6).

3.3. System Matrix

After deriving the circuit voltage equations for each Mode, the backward difference method is adopted to treat the time derivative terms and to construct the system matrix [5].

In the case of one current loop, as shown in Figs. 4(c) and (d), the system matrix can be expressed as in (7). In the case of having two circuit voltage equations as shown in Figs. 4(a) and (b), and Figs. 5 and 6, the system matrix can be written as in (8).

$$\begin{bmatrix} [S] & \{Q\} \\ \lfloor F \rfloor/\Delta t & 2R+2L_l/\Delta t \end{bmatrix} \begin{bmatrix} \{A\}^{t+\Delta t} \\ I_1^{t+\Delta t} \end{bmatrix} = \begin{bmatrix} [0] & \{0\} \\ \lfloor F \rfloor/\Delta t & 2L_l/\Delta t \end{bmatrix} \begin{bmatrix} \{A\}^{t} \\ I_1^{t} \end{bmatrix} + \begin{bmatrix} \{G\}^{t+\Delta t} \\ V_1^{t+\Delta t} \end{bmatrix} \tag{7}$$

$$\begin{bmatrix} [S] & \{Q_1\} & \{Q_2\} \\ \lfloor F_1 \rfloor/\Delta t & 2R+2L_l/\Delta t & R+L_l/\Delta t \\ \lfloor F_2 \rfloor/\Delta t & R+L_l/\Delta t & 2R+2L_l/\Delta t \end{bmatrix} \begin{bmatrix} \{A\}^{t+\Delta t} \\ I_1^{t+\Delta t} \\ I_2^{t+\Delta t} \end{bmatrix} = \begin{bmatrix} [0] & \{0\} & \{0\} \\ \lfloor F_1 \rfloor/\Delta t & 2L_l/\Delta t & L_l/\Delta t \\ \lfloor F_2 \rfloor/\Delta t & L_l/\Delta t & 2L_l/\Delta t \end{bmatrix} \begin{bmatrix} \{A\}^{t} \\ I_1^{t} \\ I_2^{t} \end{bmatrix} \begin{bmatrix} \{G\}^{t+\Delta t} \\ V_1^{t+\Delta t} \\ V_2^{t+\Delta t} \end{bmatrix} \tag{8}$$

where S is the stiffness matrix, Q and F are the matrices related to the stator winding and back-EMF, respectively. G is the forcing term by a magnet.

4. Results and Discussions

Fig. 7 shows the constructed prototype FRM and 4-switch converter with a DSP installed controller. The prototype has a six-pole stator and an eight-pole variable reluctance rotor. Fig. 8 compares the measured and the calculated current in each phase. The speed of the rotor is 1,500 rpm and the rated output is 100W. Current regulation using hysteresis current control was also performed. It should be noted that the experimental results closely match the ones of the proposed analysis method. As

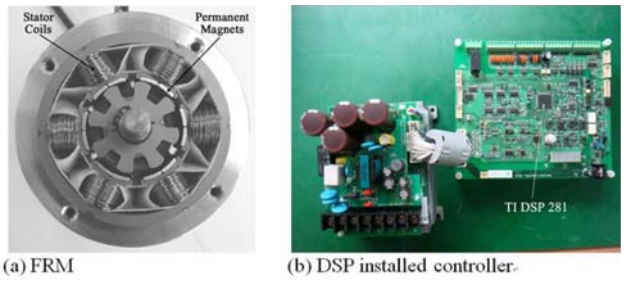

Fig. 7. (Color online) The constructed prototype FRM and DSP installed controller.

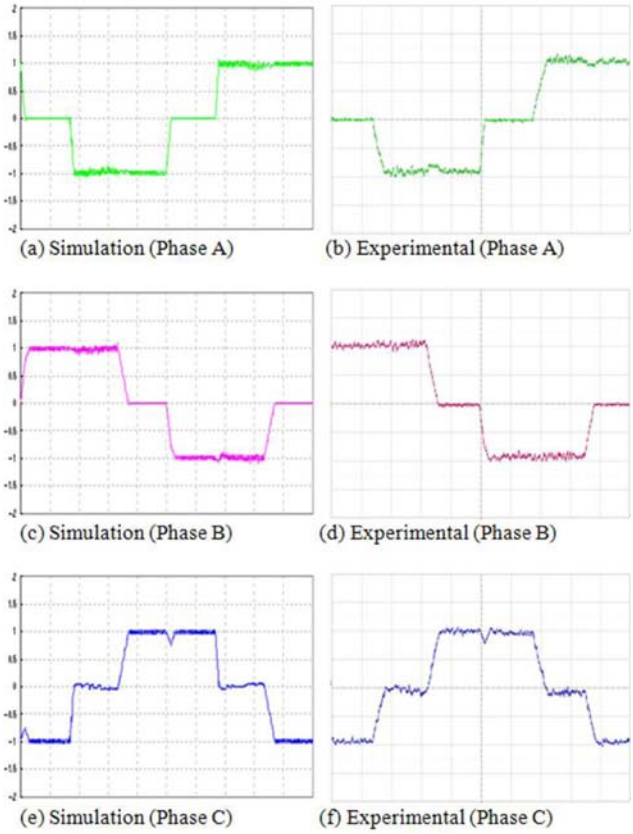

Fig. 8. (Color online) Comparison of current waveforms (0.5A/Div.).

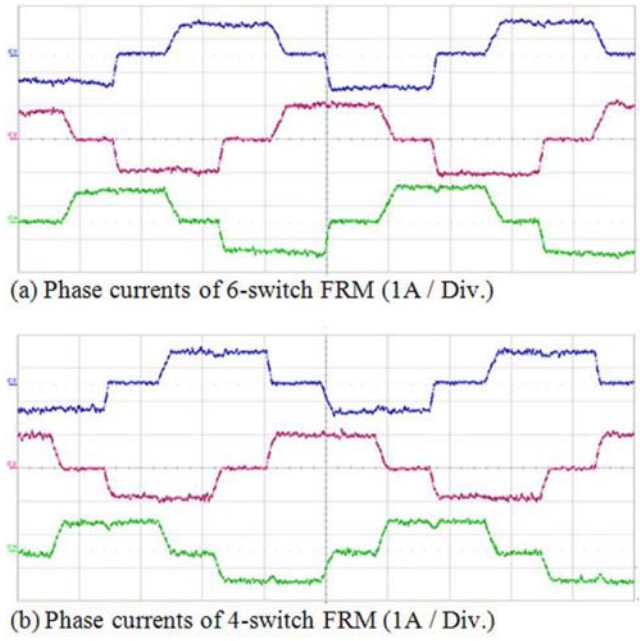

Fig. 9. (Color online) Experimental phase current waveforms.

phases A and B are activated (modes II and IV), the device is supplied with the full of dc-link voltage, so that during one PWM period in these modes the current is increased more than in the other operating modes. Moreover, independent control of phases A and B results in current ripples in phase C during the silent periods, this is caused by the difference between the phase A and phase B currents. Even though this device has more current ripples than a six-switch converter, its performance is acceptable and these problems can be further reduced by controlling the hysteresis band size. After detailed investigation of the experimental results, the authors successfully utilized the four-switch converter topology to drive a 3-phase FRM to fully show the validity of the developed direct current controlled PWM. The experimental current waveforms for 6-switch FRM and 4-switch FRM are shown in Fig. 9. The 4-switch FRM has larger current ripples with the same input voltage. However, when using the voltage-doubler and increasing the switching band the performance is similar to that of the 6-switch FRM except for a few more ripples in the current. The main reason for these ripples is the restriction of switching frequency in this converter topology.

5. Conclusions

In this paper, a 2-dimensional time-stepped voltage source finite element method taking account of back-EMF current for a 4-switch converter system was proposed. To prove the propriety of the proposed analysis method, a prototype FRM and DSP installed experimental devices were produced and tested. It was found that accurate predictions can be obtained by the proposed method. In addition, it was shown that the 4-switch converter topology with a direct current controlled PWM can be successfully utilized to drive a 3-phase FRM.

Therefore, it is expected that the proposed analysis method can be utilized for the design of FRMs with 4-switch converters.

References

[1] G. T. Kim and T. A. Lipo, IEEE Trans. Ind. Appl. **32**, 1331 (1996).
[2] J. I. Itoh and K. Fujita, IEEE Trans. Power Electron. **15**, 36 (2000).
[3] B. K. Lee, T. H. Kim, and M. Ehsani, IEEE Trans. Power Electron. **18**, 164 (2003).
[4] T. H. Kim and J. Lee, IEEE Trans. Magn. **41**, 1956 (2005).
[5] T. H. Kim, S. H. Won, and J. Lee, IEEE Trans. Magn. **42**, 1039 (2006).